Materials Science-Poland, 33(4), 2015, pp. 826-834
http://www.materialsscience.pwr.wroc.pl/
DOI: 10.1515/msp-2015-0097

DE GRUYTER OPEN

Investigation of sol-gel processed CuO/SiO_2 nanocomposite as a potential photoanode material

TENZIN TENKYONG, NEENA BACHAN, J. RAJA, P. NAVEEN KUMAR, J. MERLINE SHYLA*

Department of Physics, Energy Nanotechnology Centre (ENTeC), Loyola Institute of Frontier Energy (LIFE), Loyola College, Chennai 600 034, India

Synthesis and characterization of a highly efficient photoconductive nanocomposite comprising of two common metal oxides: copper oxide (CuO) and silicon dioxide (SiO_2) are being reported in this paper. The CuO/SiO_2 nanocomposite has been synthesized using a cost-effective and facile sol gel route. The structural, chemical and optical properties of the prepared samples have been studied using various characterization techniques. The UV-Vis analysis revealed better absorption in the case of the nanocomposite as compared to its parent materials. X-ray diffraction (XRD) analysis has been employed to determine the structural formation of the nanocomposite and the crystallite size with the use of Scherrer's formula. The photo conductivity study of the sample showed enhanced photocurrent in the case of nanocomposite as compared to its single components, thus, presenting it as a potential candidate for solar cell applications, especially as photoanode material in the dye-sensitized solar cells (DSSC).

Keywords: *sol-gel; CuO/SiO_2 nanocomposite; photoconductivity; photoanode; DSSC*

1. Introduction

Nanocomposites [1] have numerous advantages over their more limited single component counterparts due to their enhanced functionality and properties. Using of nanocomposites leads to enhancement and modification of magnetic, optical, electrical and chemical properties as compared to their individual components [2–4]. The oxides of nanoparticles are an important class of semiconductors which find applications in magnetic storage [5], solar energy transformation [6, 7], electronics [8] and catalysis [9]. In the present work, the choice of CuO as a parent material is due to the fact that it possesses excellent optical properties and high temperature superconductivity [10] which makes it a good candidate for solar cell applications. The fusion of SiO_2 with CuO was done in order to produce a nanocomposite which can overcome the limits of CuO in solar spectrum response and increase its optical absorbance. The above mentioned CuO/SiO_2 nanocomposite was prepared using the facile and efficient sol gel method which is well suited for preparing and designing devices with very specific properties [11].

2. Experimental

2.1. Synthesis of CuO nanoparticles

A solution of 0.25 g copper acetate and 1 mL dimethanol amine was added dropwise to 19 mL of isopropyl alcohol and stirred for 30 minutes. The metal oxide gel was produced by increasing pH of the solution by dropwise addition of 1 M of NH_3. The resultant solution was stirred for 24 hours and kept one day for aging. The aging process was carried out to remove particulates, if any [12]. The solution was washed with distilled water 4 to 5 times and dried at 100 °C for 24 hours in order to remove the solvents. The final step of annealing at 400 °C for 4 hours was done to remove any residual organics and stabilize the obtained nanoparticles [13].

2.2. Synthesis of SiO_2 nanoparticles

The synthesis of SiO_2 was done in a similar manner. A solution of tetraethyl orthosilicate

*E-mail: jmshyla@gmail.com

(TEOS) was added dropwise to 19 mL of isopropyl alcohol. The precursor solution preparation was followed by the steps involved in the CuO nanoparticle synthesis.

2.3. Synthesis of CuO/SiO_2 nanocomposites

The CuO/SiO_2 nanocomposite was prepared by addition of the precursor materials of CuO (copper acetate, dimethanol amine and isopropyl alcohol) to those of SiO_2 (tetraethyl orthosilicate and isopropyl alcohol). The molar ratio of the solutions was maintained at 1:1. For the preparation of the resultant solution the sol gel method was applied, leading to the formation of CuO/SiO_2 nanocomposite as shown in Fig. 1.

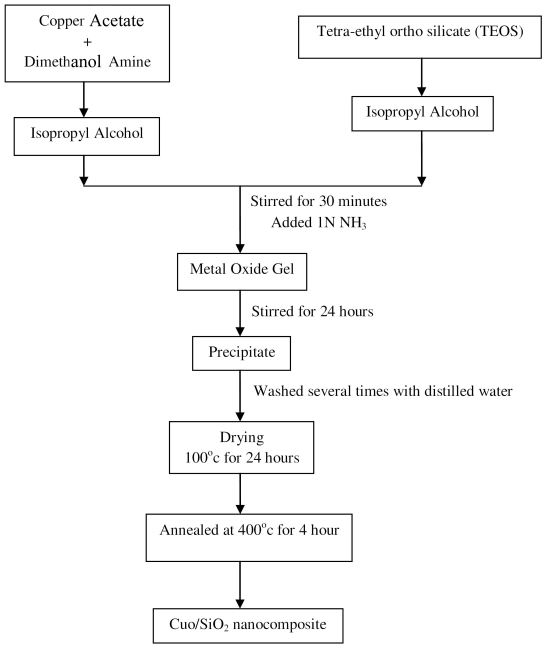

Fig. 1. Synthesis procedure of CuO/SiO_2 nanocomposite.

3. Characterization

The characterization of the sol-gel synthesised CuO, SiO_2 and CuO/SiO_2 was carried out using different techniques in order to probe their structural, chemical and optical properties. The X-ray diffraction (XRD) analysis [14] of the as-synthesised samples was carried out using Panalytical X'Pert powder diffractometer with a goniometer using CuKα as radiation source having the wavelength of 1.5405 Å. The diffraction patterns were recorded in the range of 20° to 80° with the step size of 0.02. Using the above XRD data the crystallite sizes of the particles were determined using Scherrer's formula [15, 16]. The scanning electron microscopy (SEM) [17] and the EDAX analysis of the samples were obtained by F E I Quanta FEG 200: a high resolution scanning electron microscope. Nitrogen adsorption-desorption isotherm at 74 K was obtained from ASAP 2020 Micrometrics. Surface areas were determined according to the Brunauett-Emmett-Teller (BET) model using the above data. The chemical composition of the samples was analysed using FT-IR technique [18]. The Fourier transform infrared spectra of the samples were studied using Perkin-Elmer infrared spectrophotometer and the spectrum was recorded in the wavenumber range of 500 to 4000 cm^{-1}. The UV-Vis absorption spectroscopy [19] was done by CARY 5E UV-Vis-NIR spectrophotometer. The spectra were recorded at room temperature in the range of 200 to 800 nm. The field dependent dark and photoconductivity tests of the samples were done using the experimental setup as reported by Ponniah and Xavier [20]. The dark and photo currents were measured using a Kiethley Picoammeter 6485.

4. Results and discussion

4.1. XRD analysis

The X-ray diffraction pattern of the as synthesised CuO sample is depicted in Fig. 2. It can be clearly seen that the prominent peaks of defined intensities are observed at diffraction angles of 2θ values 30.8°, 35.9°, 38.7°and 49.1° which correspond to atomic planes of (h k l) values (1 1 0), ($\bar{1}$ 1 1), (1 1 1) and ($\bar{2}$ 0 2), respectively. These peaks are consistent with the JCPDS data Card No. 48-1548 of the CuO with a monoclinic phase [21] identical to that of pure CuO [22]. The lattice parameters corresponding to

the above data card were found to be a = 4.688 Å, b = 3.422 Å and c = 5.131 Å, respectively [23]. No characteristic peaks of other impurities, such as $Cu(OH)_2$, Cu_2O or precursors used in the preparation process, are observed, indicating the formation of a pure phase of CuO. The XRD pattern of the prepared CuO/SiO_2 nanocomposites presented in Fig. 3 shows the presence of a very broad peak around 23.7° scattering angle and few peaks of CuO of very low intensities. It indicates that either the particles of CuO are of very small crystallite size, or the particles are semi-crystalline in nature [24] since the XRD pattern of prepared nanocomposite appears to be a close mimic of that of SiO_2 [25] which is amorphous.

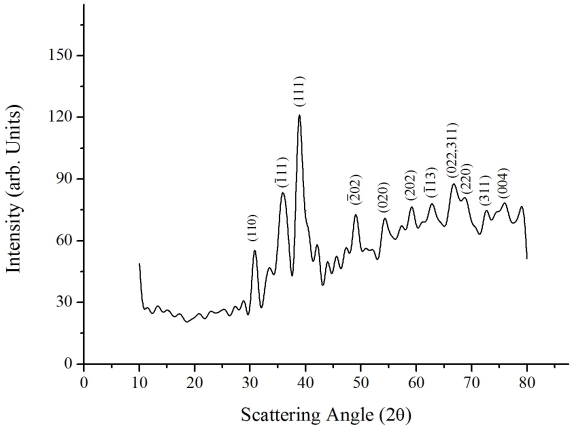

Fig. 2. XRD pattern of CuO nanoparticle.

The average crystallite size of the as-synthesized nanoparticles was estimated from XRD line broadening using Scherrer's equation. The crystallite sizes of the samples were calculated using Scherrer's equation $D = K\lambda/\beta\cos\theta$, where K is a constant (shape factor, about 0.9), λ the X-ray wavelength used (1.54060 Å), β the full width at half maximum (FWHM) of the observed peaks [26]. The crystallite sizes of the CuO nanoparticles corresponding to the calculated major peaks have been tabulated in Table 1. The average crystallite size of the CuO nanoparticles are in the range of 12 nm. The crystallite size of CuO/SiO_2 nanocomposite calculated with Scherrer's formula is found to be around 0.8 nm. This

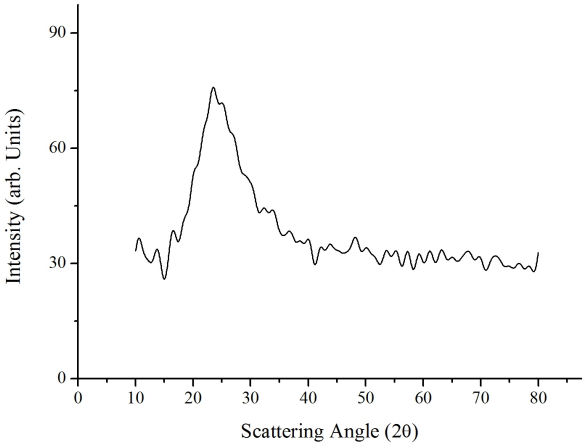

Fig. 3. XRD pattern of CuO/SiO_2 nanocomposite.

relatively low crystallite size of the nanocomposite is due to the low growth rate [27] and is consistent with our earlier reports for SiO_2 [28].

Table 1. Crystallite size for different 2θ values of CuO nanoparticles.

Diffraction angle (2θ)	Atomic planes (h k l)	FWHM (2θ)	Crystallite size (nm)
30.8	(1 1 0)	0.5904	15
35.9	($\bar{1}$ 1 1)	1.1808	8
38.7	(1 1 1)	0.4920	18
49.1	($\bar{2}$ 0 2)	1.1808	8

4.2. SEM analysis

SEM images of the CuO nanoparticle and CuO/SiO_2 nanocomposite samples are shown in Fig. 4 and Fig. 5, respectively. From the SEM image of the CuO nanoparticles it is seen that the particles occur in a form of elongated nanorod-type structure [29] and the particle sizes of the observed nanoparticles are in the range of 10 to 30 nm. The obtained nanoparticle sizes are in close proximity with the crystallite size calculated using XRD data. It is also observed that there are micro and macro pores in the sample.

The SEM image of CuO/SiO_2 nanocomposite reveals that the formed particles possess larger size than that of CuO nanoparticles. The presence of agglomerations is also observed which might be

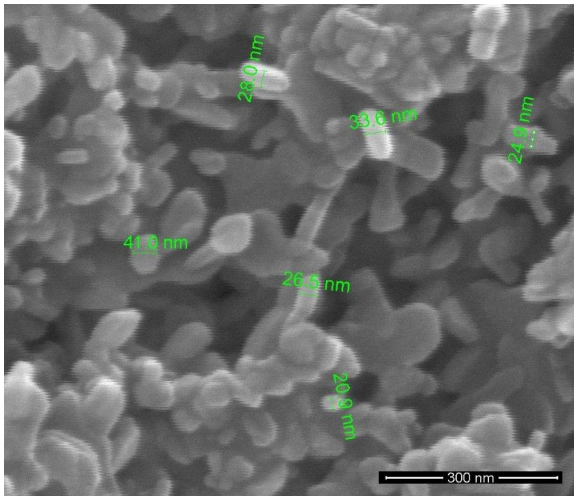

Fig. 4. SEM image of CuO nanoparticles.

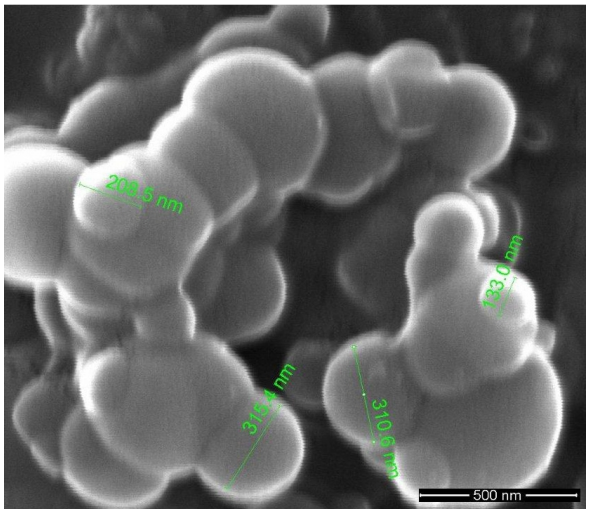

Fig. 5. SEM image of CuO/SiO_2 nanocomposite.

due to the amorphous nature of the SiO_2 as evidenced from the XRD analysis. In the literature [27], the micro- and the macro-pores have also been observed in the CuO/SiO_2 sample and the observed particle shapes were spherical in nature.

4.3. EDAX analysis

The chemical composition of the obtained CuO/SiO_2 nanocomposite was determined using energy dispersive X-ray (EDAX) analysis. In the EDAX spectrum of CuO/SiO_2 nanocomposite shown in Fig. 6, the prominent peaks of oxygen (O) and silicon (Si) are observed with few subsided peaks of copper (Cu) which reveals that the obtained CuO/SiO_2 nanocomposite is mainly composed of Si and O with traces of Cu [30]. The observed data confirm the presence of a small amount of CuO in the CuO/SiO_2 which is again in accordance with the XRD result. The amount of each element present in the CuO/SiO_2 nanocomposite is listed in Table 2.

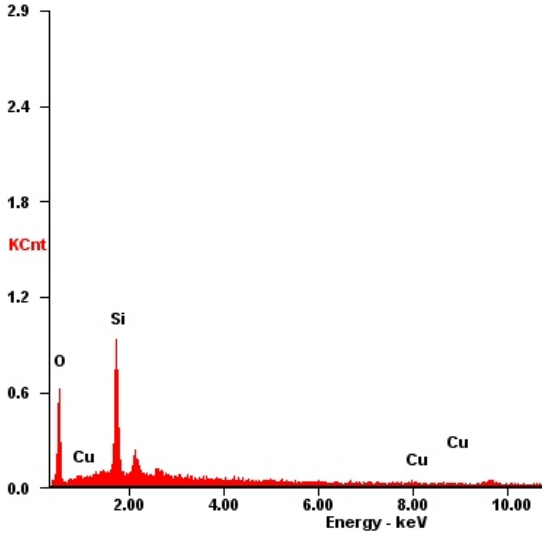

Fig. 6. EDAX analysis of CuO/SiO_2 nanocomposite.

Table 2. Elemental analysis of the CuO/SiO_2 nanocomposite sample.

Element	Weight %	Atomic %
Oxygen (O)	65.79	77.82
Silicon (Si)	31.90	21.49
Copper (Cu)	02.31	00.69

4.4. BET analysis

The specific surface area and pore structure of the as-prepared CuO nanoparticles and CuO/SiO_2 nanocomposites were investigated by nitrogen adsorption-desorption isotherm. Fig. 7 and Fig. 8 show the nitrogen adsorption-desorption isotherm and Fig. 9 and Fig. 10 BET surface area plot. It is clear that both the samples exhibit the type IV

isotherm of H3 type hysteresis loop for the relative pressure P/P_0 in the range of 0.6 to 1 according to Brunauer-Deming-Deming-Teller (BDDT) classification [31, 32] revealing the characteristic properties of mesoporous materials and the presence of mesopores (2 to 50 nm) [33]. The specific surface area estimated by Brunauer-Emmett-Teller method for both the samples are tabulated in Table 3. Upon formation of the composite with SiO_2 a decrease in the specific surface area of CuO is observed. This may be due to the agglomerations occurring in the presence of SiO_2 which is also inferred from XRD analysis. In the nanocomposite sample, copper oxide nanoparticles are coated with SiO_2 nanoparticles. Therefore, when the surface area of CuO/SiO_2 nanocomposites is measured, it is possible that its size is dominantly determined by the surface properties of the amorphous SiO_2 rather than CuO [34]. For this reason, a relatively low specific surface of the CuO/SiO_2 nanocomposites is apparent compared to that of CuO nanoparticles. However, the mesoporous CuO/SiO_2 nanocomposites possess a specific surface area considerably larger than that of the as-synthesised SiO_2 nanoparticles [28].

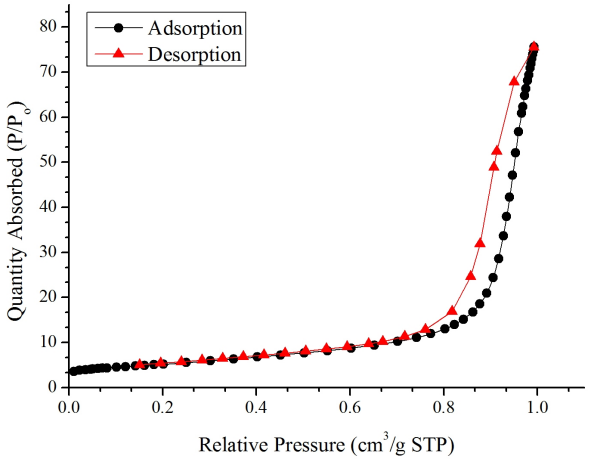

Fig. 7. Nitrogen adsorption-desorption isotherm of CuO nanoparticles.

4.5. FT-IR analysis

The IR spectra of the samples have been scanned in the region of 4000 to 450 cm^{-1}. The IR spectrum of the copper (II) oxide (CuO) consists

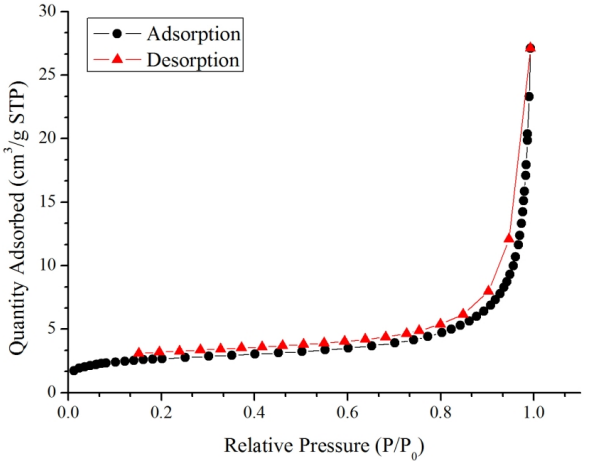

Fig. 8. Nitrogen adsorption-desorption isotherm of CuO/SiO_2 nanocomposite.

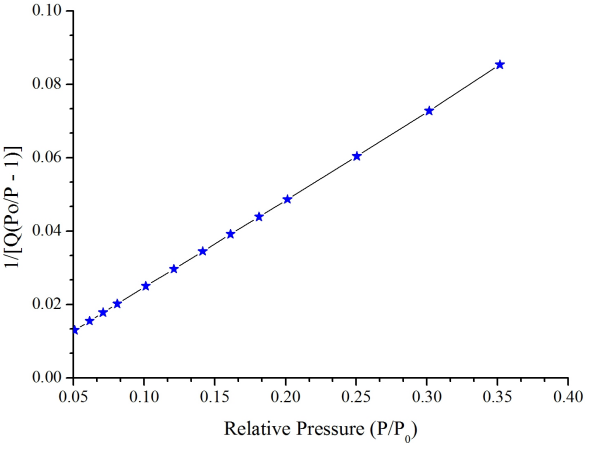

Fig. 9. BET surface area plot of CuO nanoparticles.

of characteristic peaks at 3435 cm^{-1}, 1633 cm^{-1}, 1384 cm^{-1}, 1033 cm^{-1}, 606 cm^{-1}, 511 cm^{-1} and 457 cm^{-1}.

As shown in Fig. 11 the CuO nanoparticles exhibit broad absorption bands between 2800 and 4000 cm^{-1}, mainly ascribed to OH– and C–O groups on the surface of the CuO nanostructures [35]. The absorption peaks at 457 cm^{-1}, 511 cm^{-1} and 606 cm^{-1} may be associated with the characteristic stretching vibrations of Cu–O [36]. This confirms that the CuO phase is formed in conformity with the XRD data. The absorption peaks at 3435 and 1633 cm^{-1} are due to the presence of O–H stretching and bending vibrations [37] which is probably due to the

Table 3. Physical properties of the samples obtained from BET analysis.

Sample	S_{BET} (m^2/g)	V_{tot} (cm^3/g)
CuO	18.13	0.11
SiO_2^*	5.71	0.0095
CuO/SiO_2	9.93	0.041

S_{BET}: BET surface area. V_{tot}: single point total pore volume. *The SiO_2 data have already been reported in our previous paper [28].

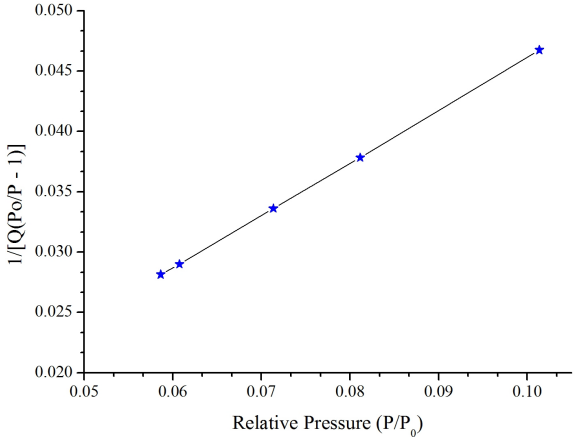

Fig. 10. BET surface area plot of CuO/SiO_2 nanocomposite.

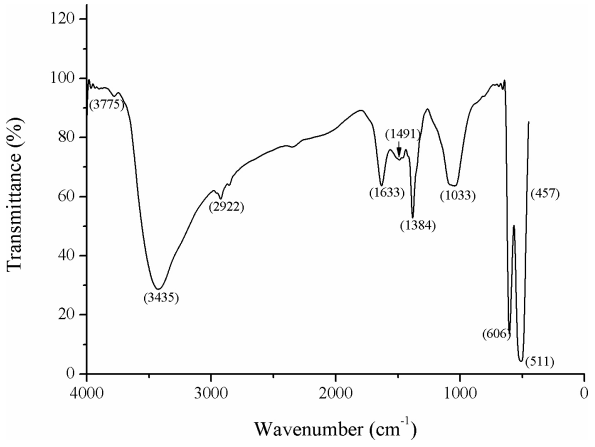

Fig. 11. FT-IR spectrum of CuO nanoparticles.

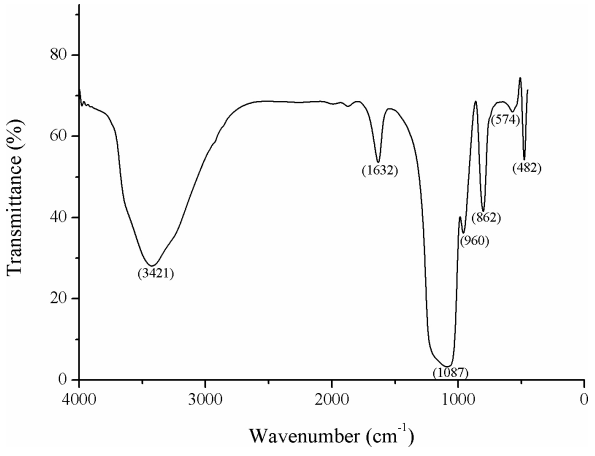

Fig. 12. FT-IR spectrum of CuO/SiO_2 nanocomposite.

fact that the spectra were not recorded *in situ* and some re-adsorption of water from the ambient atmosphere occurred. The FT-IR spectrum of CuO/SiO_2 (Fig. 12) shows the typical silicate absorption peaks at about 1087 (with a shoulder around 1400 cm^{-1}), 862, 574 and 482 cm^{-1} attributable to Si–O–Si bending and stretching vibrations [38]. The CuO/SiO_2 nanocomposite also shows a broad band at about 3421 cm^{-1} and a band at 1632 cm^{-1}. The former is due to surface hydroxyl groups and adsorbed water, while the later can be assigned to water only. The absorption peak observed at 960 cm^{-1} for CuO/SiO_2 is possibly due to the overlapping of Si–OH bond [39] with the bending vibration of Si–O bond. The intensity of this band is taken as an indication of heterogeneity (presence of CuO) in the mixed oxides [40]. The results obtained from both the FT-IR spectra are in good agreement with the XRD results.

4.6. UV-Vis absorption spectroscopy

The absorption spectra of the as-synthesized CuO nanoparticles and CuO/SiO_2 nanocomposites are shown in Fig. 13 and Fig. 14, respectively. The absorption peaks present at 256 nm in both the samples are attributed to Cu^{2+} in the zeolite structure [41]. Also the existence of absorption band at and around 800 nm in these samples are due to the presence of Cu^{2+} ion [42] and are related to the electron transmission of the d orbitals. The above two observations clearly explain the presence of the copper (II) ions in both the samples and more importantly the presence of copper (II) ions in the internal position of silica matrix [43] in the CuO/SiO_2 nanocomposite sample. But it is also observed that in the case of nanocomposite sample

there is a slight decrease in the absorption in visible region as compared to the CuO nanoparticle sample which could be due to the low concentration of CuO in the composite sample [44] as well as the transmitting nature of the SiO_2.

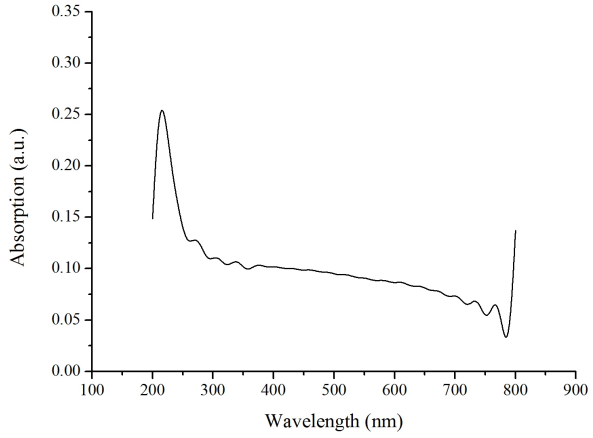

Fig. 13. UV-Vis absorption spectrum of CuO nanoparticles.

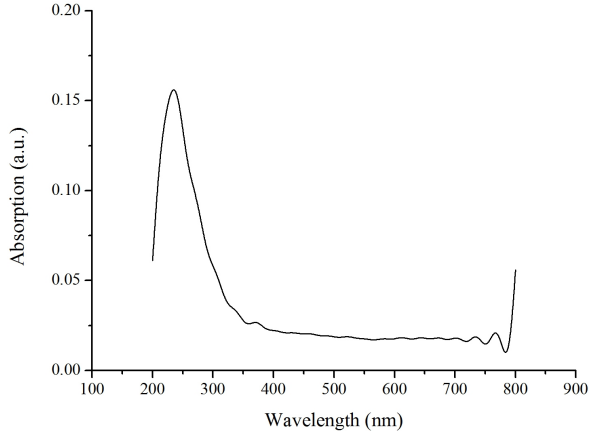

Fig. 14. UV-Vis absorption spectrum of CuO/SiO_2 nanocomposite.

4.7. Field dependent dark and photoconductive currents

For the field dependent dark and photoconductive current measurements, the samples in the form of pellets were attached to a microscopic glass slide and two electrodes of thin copper wire (0.14 mm diameter) were fixed using silver paint. The ends of the copper wires were connected to DC power supply through a picoammeter as shown in Fig. 15. The applied field was varied and the corresponding current in the circuit was measured. To measure the photocurrent, the same setup was retained but with the light from a 100 W halogen lamp illuminating the sample. The field dependent dark and photocurrent characteristics of CuO nanoparticles are shown in Fig. 16. The plots indicate a linear increase of current in the dark and visible light-illuminated conditions with an increase in the applied field, depicting the ohmic nature [45] of the contacts.

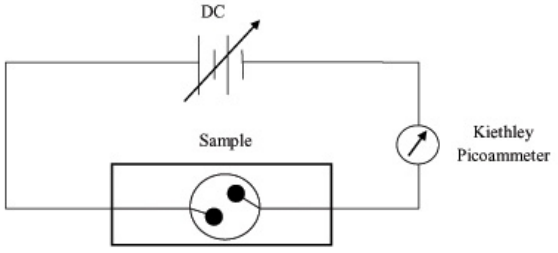

Fig. 15. Experimental setup for field dependent photoconductivity test.

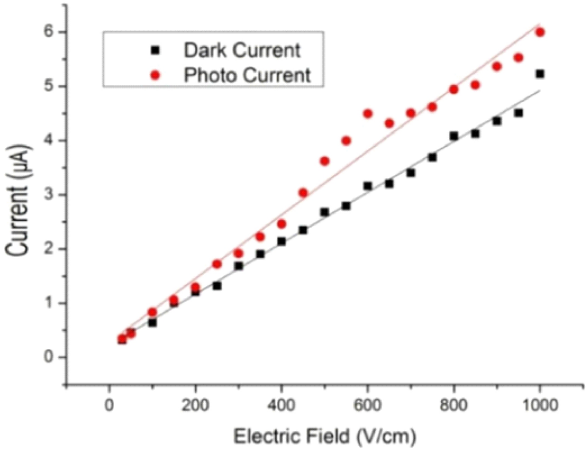

Fig. 16. Field dependent dark and photoconductive currents of CuO nanoparticles.

The dark and photoconductivity characteristics of CuO/SiO_2 nanocomposites presented in Fig. 17 also evidence the ohmic nature of the contact by gradual increase in current with the increase in the applied field. The dark and photocurrent

Table 4. Dark and photo current values at a fixed applied field.

Fixed applied field	CuO		SiO_2^*		CuO/SiO_2	
	I_D	I_P	I_D	I_P	I_D	I_P
600 $V \cdot cm^{-1}$	0.01 μA	0.02 μA	0.003 μA	0.003 μA	0.5 mA	0.8 mA

*The SiO_2 data has been experimentally measured and reported in our previous paper [28].

values of the samples calculated for a fixed field of 600 V/cm are tabulated in Table 4.

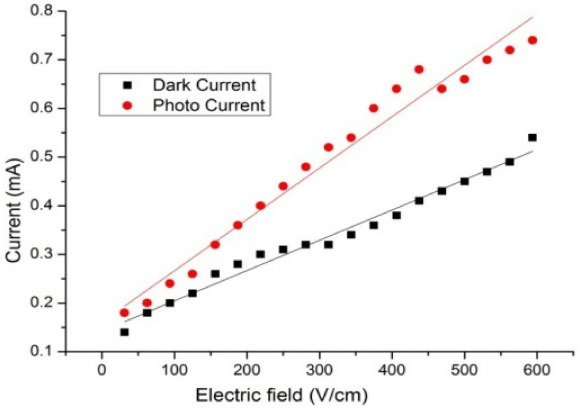

Fig. 17. Field dependent dark and photoconductive currents of CuO/SiO_2 nanocomposite.

The resistivity of the CuO and SiO_2 nanoparticles as well as CuO/SiO_2 nanocomposite has been measured from the inverse of slope of the I-V curve and is found to be approximately 0.8×10^3 MΩ·cm, 1.6×10^3 MΩ·cm and 0.2×10^3 kΩ·cm for dark conductivity and 0.5×10^3 MΩ·cm, 1.6×10^3 MΩ·cm and 0.1×10^3 kΩ·cm in case of photoconductivity, respectively. In comparison with the parental counterpart CuO, there is a decline in resistivity by an order of about 10^3 in both the dark and the illuminated condition thereby confirming the enhanced conducting nature of the synthesized nanocomposite.

The analysis of the said values reveals that the field dependent dark and photocurrent of the nanocomposite are larger than those of the CuO nanoparticle sample and also that of SiO_2 samples made in our lab earlier and already reported in the literature [28], essentially indicating enhanced photoconductivity and probable photon conversion efficiency of the CuO/SiO_2 nanocomposite.

5. Conclusions

Nanocomposites of sol-gel processed CuO and SiO_2 nanoparticles were synthesized and characterized using various techniques. The XRD and SEM analyses show that the particle size of the CuO nanoparticle is relatively small and its role in the nanocomposite is minimal as compared to its counterpart SiO_2. The FT-IR spectra reveal corresponding chemical bonding between the molecules and the formation of CuO, SiO_2 and CuO/SiO_2 phases in respective cases. The BET studies of the samples reveal the presence of mesopores and decrease in the surface of the nanocomposite as compared to pure CuO nanoparticles. CuO/SiO_2 nanocomposite exhibits enhanced dark and photoconductivity currents in comparison with that of its individual components CuO and SiO_2. Hence, it can be concluded from this study that there is a significant change in the structural, surface and chemical properties and relative enhancement in the transport properties of the material upon formation of nanocomposite. Thus, the synthesized CuO/SiO_2 nanocomposite which is equipped with improved properties could be proposed as a potential substitute for its counterpart nanoparticles and an independent contender for applications in the field of solar cell and sensors.

Acknowledgements

The authors acknowledge the Loyola Institute of Frontier Energy (LIFE), the Loyola College, Chennai 600034, for the financial and technical support extended towards this project.

References

[1] AJAYAN P.M., SCHADLER L.S., BRAUN P.V., *Nanocomposites Science and Technology*, Wiley & Sons, New York, 2003.

[2] KIM H., ACHERMANN M., BALET L.P., HOLLINGSWORTH J.A., KLIMOV V.I., *J. Am. Chem. Soc.*, 127 (2005), 544.

[3] HINES M.A., GUYOT SIONNEST P., *J. Phys. Chem.*, 100 (1996), 468.
[4] TOHIDI, HOSSEIN, GRIGORYAN, GARNIK, SARKEZIYAN, *Iran. J. Chem. Chem. Eng.*, 29 (2010), 27.
[5] HUANG X., FU Z., YANG X., SUN Z., ZHONG M., YI Y., TANG Y., WANG C., *J. Porous Mat.*, 21 (2014), 9.
[6] ALI A., JO J., YANG Y. J., CHOI K. H., *Appl. Phys. A-Mater.*, 114 (2014), 323.
[7] NAAZEERUDDIN M.K., KAY A., GRATZEL M., *J. Am. Chem. Soc.*, 155 (1993), 6832.
[8] VAYSSIERES L., *Appl. Phys. A-Mater.*, 89 (2007), 1.
[9] CAO J., WANG Y., SHI J., SUN G., ZHANG Z., *J. Porous Mat.*, 18 (2011), 667.
[10] NADDAF M., MRAD O., AL-ZIER A., *Appl. Phys. A-Mater.*, 115 (2014), 1345.
[11] LIVAGE J., HEMRY M., SANCHEZ C., *Prog. Solid State Ch.*, 18 (1988), 259.
[12] ZHU Y. F., ZHANG L., GAO C, CAO L. L., *J. Mater. Sci.*, 35 (2000), 4049.
[13] AGUADO J., VAN RAFAEL G., MARIA-JOSE L-M., JAVIER M., *Appl. Catal. A-Gen.*, 312 (2006), 202.
[14] CHATTERJEE S.K., *X-ray Diffraction: Its Theory and Application*, PHI, India, 2010.
[15] HALL B.D., ZANCHET D., UGARTE D., *J. Appl. Crystallogr.*, 33 (2000), 1335.
[16] MONSHI A., FOROUGHI R.M., *World J. Nano Sci. Eng.*, 2 (2012), 154.
[17] GENG Z.R., LI Y., YAN R. J., WANG C.B., LING X.M., *Adv. Mater. Res.*, 834 – 836 (2013), 50.
[18] JOHN COATES, *Interpretation of Infrared Spectra, A Practical Approach*, in: MEYERS R.A. (Ed.), *Encyclopedia of Analytical Chemistry*, John Wiley & Sons Ltd., Chichester, 2000, p. 10815.
[19] OWEN T., *Fundamentals of UV visible spectroscopy*, Agilent Technology, Germany, 2000.
[20] PONNIAH D., XAVIER F., *Phys. Biol.*, 20 (2007), 392.
[21] ETHIRAJ A. S., KANG D. J., *Nanoscale Res. Lett.*, 7 (2012), 70.
[22] BEHERA M., GIRI G., *Mater. Sci.-Poland*, 32 (2014), 702.
[23] SAHAY R., KUMAR P.S., ARAVINDHAN V., LING W.C., *J. Phys. Chem. C*, 116 (2012), 18087.
[24] YEH C.L., YEH S.H., MA H.K., *Powder Technol.*, 145 (2004), 1.
[25] SENKEVICH J. J., DESU S. B., *Appl. Phys. A-Mater.*, 70 (2000), 541.
[26] CASTRO A.L., NUNES M.R., *Solid State Sci.*, 10 (2008), 602.
[27] LI J., VIZKELETHY G., REVESZ P., MAYER J.W., TU K.N., *J. Appl. Phys.*, 69 (1991), 1020.
[28] KUMAR A.D., XAVIER F.P., SHYLA M.J., *Appl. Nanosci.*, 2 (2012), 429.
[29] DHANASEKARAN V., SOUNDARAM N., CHANDRAMOHAN R., *New J. Chem.*, 38 (2014), 2327.
[30] AHMED N.M., SELIM M.M., *Anti-Corros. Method. M.*, 57 (2010), 133.
[31] YU H., LUI R., WANG X., WANG P., YU J., *Appl. Catal. B-Environ.*, 111 (2012), 326.
[32] ZHANG S., ZHANG C., MAN Y., ZHU Y., *J. Solid State Chem.*, 179 (2006), 62.
[33] WANG X., LI S., YU H., YU J., *J. Mol. Catal. A-Chem.*, 334 (2011), 52.
[34] STENGL V., BAKARDJIEVA S., GRYGAR T. M., BLUDSKA J., KORMUNDA M., *Chem. Cent. J.*, 7 (2013), 41.
[35] THEKKAE PADIL V.V., ČERNÍK M., *Int. J. Nanomed.*, 8 (2013), 889.
[36] RAHMAN A., ISMAIL A., JUMBIANTI D., MAGDALENA S., *Indian J. Chem. B*, 9 (2009), 355.
[37] AZAM A., AHMED A.S., OVES M., KHAN M.S., HABIB S.S., MEMIC A., *Int. J. Nanomed.*, 7 (2012), 6003.
[38] CRUZA DA R.S., SILVAA DE J.M., ARNOLDA U., SERCHELI SCHUCHARDT M.S., *J. Braz. Chem. Soc.*, 13 (2002), 170.
[39] NEUMANN R., LEVIN-ELAD M., *J. Catal.*, 166 (1997), 206.
[40] MILLER J.B., RANKIN S.E., KO E.I., *J. Catal.*, 148 (1994), 673.
[41] MORETTI G., DOSSI C., FUSI A., RECCHIA S., PSARO R., *Appl. Catal. B-Environ.*, 1 (1999), 67.
[42] MARTINEZ J.R., RUIZ F., VOROBIEV Y.V., GONZALEZ J., *J. Chem. Phys.*, 109 (1998), 7511.
[43] WANG Z., LUI Q., YU J., WU T., WANG G., *Appl. Catal. A-Gen.*, 239 (2003), 87.
[44] JIMENEZ J.A., *Appl. Phys. A-Mater.*, 114 (2014), 1369.
[45] DHAR S., CHAKRABARTI S., *Semicond. Sci. Tech.*, 11 (1996), 1231.

Received 2015-02-17
Accepted 2015-08-20